Ore Geology Reviews 187 (2025) 106952

Contents lists available at ScienceDirect

Ore Geology Reviews

journal homepage: www.elsevier.com/locate/oregeorev

Distribution pattern of hydrogenetic cobalt-rich nodules in the Pacific Ocean and peripheral seas

Xiangwen Ren [a,b,*], Ying Liu [c], Shijuan Yan [a,b], Yuxue Zhang [a], Chunhua Han [d], Xuefa Shi [a,b]

[a] Key Laboratory of Marine Geology and Metallogeny, First Institute of Oceanography, Ministry of Natural Resources, Qingdao 266061, China
[b] Laboratory for Marine Geology, Laoshan State Laboratory, Qingdao 266237, China
[c] China Deep Ocean Affairs Administration, Beijing 100860, China
[d] National Marine Data and Information Service, Ministry of Natural Resources, Tianjin 300012, China

ARTICLE INFO

Keywords:
Hydrogenetic nodules
Cobalt
Binary logistic regression
Kernel density
Pacific Ocean

ABSTRACT

Polymetallic nodules are one of the most promising mineral resources available for deep-sea exploitation. The cobalt content in hydrogenetic nodules is comparable to that found in terrestrial hydrothermal and volcanic polymetallic cobalt deposits, identifying these nodules as a significant potential source of cobalt from the ocean floor. Understanding the spatial distribution pattern of hydrogenetic cobalt-rich nodules is therefore essential for advancing the development of deep-sea cobalt resources. This study concentrates on the Pacific Ocean and its peripheral seas. Using data on ore-controlling parameters such as global marine sediment thickness, calcium carbonate ($CaCO_3$) concentration in surface sediments, primary productivity, near-bottom current velocity, water depth and elevation, and near-bottom dissolved oxygen levels, along with information on Pacific polymetallic nodule types, the spatial occurrence of hydrogenetic cobalt-rich nodules was estimated through a combination of binary logistic regression and kernel density analysis. The findings reveal that both mineralization principles and the spatial resolution of ore-controlling datasets significantly influence predictive accuracy. The results demonstrate that hydrogenetic cobalt-rich nodules in the Pacific Ocean are primarily located in low-latitude zones of the western Pacific, including the Mariana Basin, the Philippine Basin, the northern Central Pacific Basin, and the northern Southwest Pacific Basin. Additional occurrences have been identified near 60 degrees south latitude in the Southern Ocean. Multiple environmental and geological parameters govern the spatial distribution of these nodules, though the theoretical ore-control framework and statistical outputs are not entirely aligned. Among the controlling parameters, sediment thickness and primary productivity emerge as the dominant factors affecting the predicted distribution of hydrogenetic cobalt-rich nodules.

1. Introduction

Polymetallic nodules are formed through the precipitation of ferromanganese oxides and hydroxides around various nuclei such as fish teeth and rock debris, etc (Hein et al., 2020; Kuhn et al., 2017). These nodules contain abundant metal elements including cobalt, nickel, manganese, copper, molybdenum, lithium, rare earth elements, and gallium, and occur extensively on the seafloor at depths ranging from 3500 to 6500 m (Hein et al., 2020; Kuhn et al., 2017). The total global resource of polymetallic nodules is estimated to be about 210 billion tons (Mizell et al., 2022). As an emerging source of metal ores, their formation is primarily governed by hydrogenetic and diagenetic processes. Hydrogenetic precipitation introduces higher concentrations of cobalt and rare earth elements into the nodules, whereas diagenetic processes predominantly enrich nickel and copper (Kuhn et al., 2017). This distinction is evident in hydrogenetic nodules from the Cook Islands Exclusive Economic Zone (EEZ), which exhibit an average cobalt content of 0.375 % (Hein et al., 2015), surpassing that of diagenetic nodules from the Peru Basin (0.0475 %) and mixed hydrogenetic-diagenetic nodules from the Clarion-Clipperton Zone (CCZ) (0.1918 %) (Mizell et al., 2022). The estimated volume of hydrogenetic nodules in the Cook Islands EEZ reaches 8.86 billion tons, containing approximately 35.3 million tons of cobalt (Hein et al., 2015), a figure comparable to the global terrestrial cobalt reserve of 11 million tons (USGS, 2024). The combination of elevated cobalt grades and significant resource quantities underscores the potential of hydrogenetic cobalt-rich nodules as an

* Corresponding author at: First Institute of Oceanography, Ministry of Natural Resources, 6 Xianxialing Road, Qingdao 266061, China.
E-mail address: renxiangwen@163.com (X. Ren).

https://doi.org/10.1016/j.oregeorev.2025.106952
Received 19 January 2025; Received in revised form 14 October 2025; Accepted 15 October 2025
Available online 21 October 2025

important source of cobalt ore.

The accumulation of cobalt in hydrogenetic nodules originates from a dynamic adsorption process involving cobalt ions. In seawater, Mn^{2+} and $Fe^{2+}$are oxidized to form Mn^{4+} and Fe^{3+} colloids (Koschinsky and Hein, 2003). These colloidal particles subsequently precipitate as amorphous ferrihydrite (FeOOH) and cryptocrystalline Fe-vernadite (δ-MnO_2), which gradually aggregate around a central nucleus to produce nodules (Koschinsky and Hein, 2003). The δ-MnO_2 phase possesses

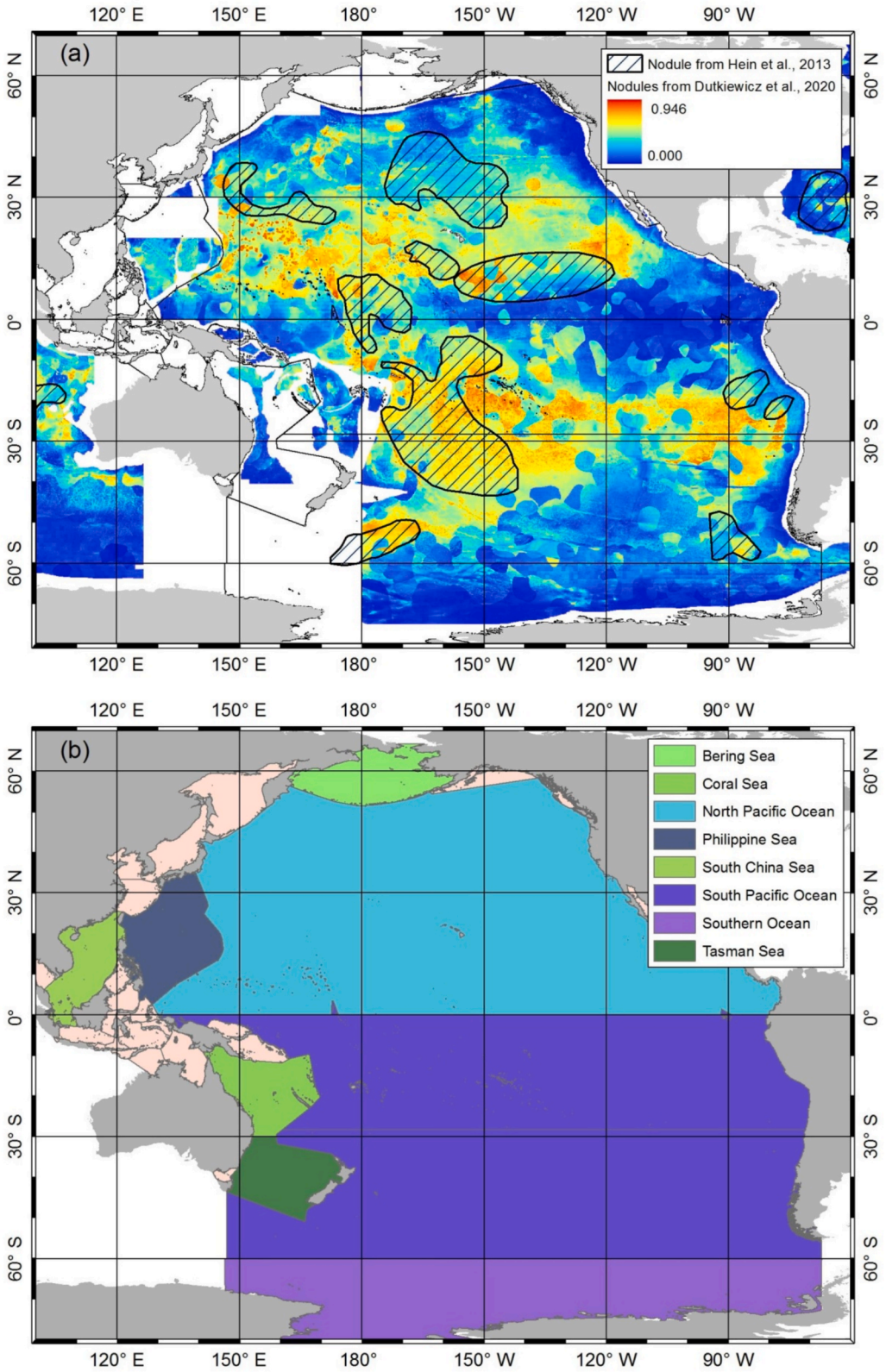

Fig. 1. The Pacific Ocean and peripheral seas and nodule distribution (a) the nodule distribution range delineated by Hein et al. (2013), and predicted by Dutkiewicz et al. (2020); (b) the scopes of oceans and seas from Flanders Marine Institute.(2018).

a large specific surface area (Ren et al., 2023), enabling efficient adsorption of Co^{2+} ions from ambient seawater. The adsorbed Co^{2+} is then oxidized to Co^{3+} by δ-MnO_2 (Manceau et al., 1997), promoting the continuous accumulation of cobalt within hydrogenetic nodules under oxic marine conditions and in regions with minimal sediment deposition (Kuhn et al., 2017).

Andreev (2020) classified deep-sea ferromanganese deposits into five distinct geochemical categories: (1) the 2Co'' type characterized by Ni + Cu contents of 0.3–0.7 %, Co concentrations exceeding 0.4 %, and Mn ranging from 14.0–24.0 %; (2) the Co type with Ni + Cu levels of 0.3–0.7 %, Co below 0.4 %, and Mn between 15.0–21.0 %; (3) the Ni–Cu–Co type containing Ni + Cu of 0.7–1.7 %, Co below 0.4 %, and Mn ranging from 21.35–27.0 %; (4) the Ni–Cu type defined by Ni + Cu greater than 1.7 %, Co below 0.4 %, and Mn between 25.0–33.0 %; and (5) the Mn type with Ni + Cu of 0.7–2.0 %, Co between 0.02–0.14 %, and Mn ranging from 33.0–47.0 %.Using the reserves-weighted average cobalt grade of 0.23 %for terrestrial hydrothermal and volcanic polymetallic deposits (Bouabdellah et al., 2016; Zou et al., 2018; Wang et al., 2017; Peter and Scott, 1997; Prokin and Buslaev, 1998; Peltonen et al., 2008; Jiao et al., 2009; Herrington et al., 2005; Yu et al., 2014; Williams and Pollard, 2001; Zhu et al., 2014) as a benchmark, the cobalt concentrations in the Co and 2Co'' types of deep-sea ferromanganese deposits defined by Andreev (2020) are comparable to those of land-based hydrothermal and volcanic cobalt-bearing deposits. This indicates that the Co and 2Co'' types possess strong potential as cobalt resources. According to Andreev's (2020) classification, these two types of deep-sea ferromanganese deposits are primarily associated with nodules and crusts located in the southern and western regions of the Pacific Ocean, where hydrogenetic nodules with elevated cobalt contents have been reported (Hein et al., 2015; Mizell et al., 2022).

The Pacific Ocean hosts the world's largest concentration of polymetallic nodules, with notable accumulations in the CCZ, the Peru Basin, the Cook Islands Exclusive Economic Zone, and the western Pacific. These regions contain predominantly hydrogenetic–diagenetic, diagenetic, and hydrogenetic nodules (Hein et al., 2020). Since 1965, numerous investigations have examined the spatial distribution of these Pacific deposits. Mero (1965) classified the Pacific Ocean into four distinct zones based on the concentrations of transition elements within the nodules: Zone A, characterized by iron-rich nodules; Zone B, by manganese-rich nodules; Zone C, by nickel and copper-rich nodules; and Zone D, by cobalt-rich nodules. Zone D primarily occupies the low-latitude regions of the central Pacific. Cronan (1967) further observed that nodules in the western and southern Pacific display higher cobalt contents than those in the eastern part. The Mineragenetic Map of the World Ocean (Александров et al., 2009) indicates that Co and 2Co types of ferromanganese deposits are mainly distributed in the Northwest Pacific Basin and the Penrhyn Basin. Hein et al. (2013) mapped the global extent of seafloor polymetallic nodules, showing that they predominantly occur in deep-sea basins. However, subsequent predictions by Dutkiewicz et al. (2020) revealed differences from the boundaries delineated by Hein et al. (2013), particularly in several deep-sea basins such as the Pigafetta Basin (Fig. 1a). Overall, studies specifically addressing the spatial distribution of cobalt-rich nodules as an independent category remain scarce. The present investigation targets the Pacific Ocean and its peripheral seas, employing an integrated approach combining binary logistic regression and kernel density estimation to analyze the distribution pattern of hydrogenetic cobalt-rich nodules and to delineate the Area for Potential Resource Assessment (APRA).

2. Materials and methods

2.1. Data sources

The boundaries of the Pacific Ocean and its peripheral seas in this research are delineated according to the IHO Sea Areas (version 3) from the Flanders Marine Institute (Flanders Marine Institute, 2018). The study area includes the South Pacific Ocean, North Pacific Ocean, Southern Ocean, Philippine Sea, Coral Sea, South China Sea, Tasman Sea, and Bering Sea, covering approximately 94.2 % of the total investigated region (Fig. 1b). The global ore-controlling parameters include near-bottom current velocity (Sulpis et al., 2018), marine sediment thickness (Straume et al., 2019), global primary productivity across land and ocean (Oregon State University, 2020), calcium carbonate($CaCO_3$) concentration in surface sediments (Sulpis et al., 2018), bathymetric and elevation data (General Bathymetric Chart of the Oceans, 2013), and near-bottom dissolved oxygen levels at 500 m depth (World Ocean Circulation Experiment, 2020). The global polymetallic nodule dataset comprises 8141 data entries describing the concentrations of Mn, Fe, Co, Ni, and Cu in nodules. These data primarily include 1736 records from the Scripps Institution of Oceanography (Frazer and Fisk, 1981), 1270 records from the dataset compiled by Monget et al. (1976), and 2736 entries from the International Seabed Authority's polymetallic nodule database (International Seabed Authority, 2010). In addition, 54 data points from the Cook Islands Exclusive Economic Zone (Hein et al., 2015) and 42 data points from the Peru Basin (von Stackelberg, 1997) are incorporated. The dataset also contains 8117 records specifying geochemical types of polymetallic nodules, consisting of 4265 samples with elemental compositions of Mn, Fe, Co, Ni, and Cu, along with 3852 samples classified by geochemical type obtained from VNIIOceanography (Andreev et al., 2004).

2.2. Method

2.2.1. Method flow chart

To integrate the strengths of data-driven statistical analysis (e.g., Dutkiewicz et al., 2020) and geological interpretation (e.g., Hein et al., 2013), this study employed a combined approach using binary logistic regression and kernel density estimation. Binary logistic regression serves as a statistical modeling technique that establishes the relationship between a binary outcome variable (presence or absence of hydrogenetic cobalt-rich nodules) and multiple predictor variables (controlling factors of such nodules). However, this method may introduce overfitting. In contrast, kernel density estimation is a non-parametric technique that estimates the probability density function of a random variable (distribution of hydrogenetic cobalt-rich nodules in this case) but excludes areas lacking sampling data. To enhance prediction reliability, the outputs of binary logistic regression and kernel density estimation were intersected in the final analysis.

The methodological framework for delineating the APRA of hydrogenetic cobalt-rich nodules in the Pacific Ocean is presented in Fig. 2 and comprises three main stages: (I) binary logistic regression-based distribution analysis, (II) kernel density-based distribution analysis, and (III) APRA delineation. The first stage includes three procedures: (I-1) data preparation, (I-2) establishment of the binary logistic regression equation, and (I-3) generation of the predicted distribution of cobalt-rich nodules using the regression model. The second stage involves (II-1) data preparation, (II-2) kernel density analysis with threshold optimization, and (II-3) calculation of the cobalt-rich nodule distribution based on kernel density estimation. The final stage focuses on (III-1) deriving the intersection of the predicted distributions from steps I-3 and II-3, followed by (III-2) determining the APRA distribution of cobalt-rich nodules. This integrated step accounts for both high-probability occurrence zones and the need for spatial precision in delineating potential cobalt-rich areas.

2.2.2. Binary logistic regression study of hydrogenetic cobalt-rich nodule distribution

I-1 Data preparation

The "Extract by Mask" function in ArcGIS was employed to isolate data within the designated study region, including near-bottom current velocity, sediment thickness, primary productivity, $CaCO_3$ concentration in surface sediments, water depth, dissolved oxygen levels in

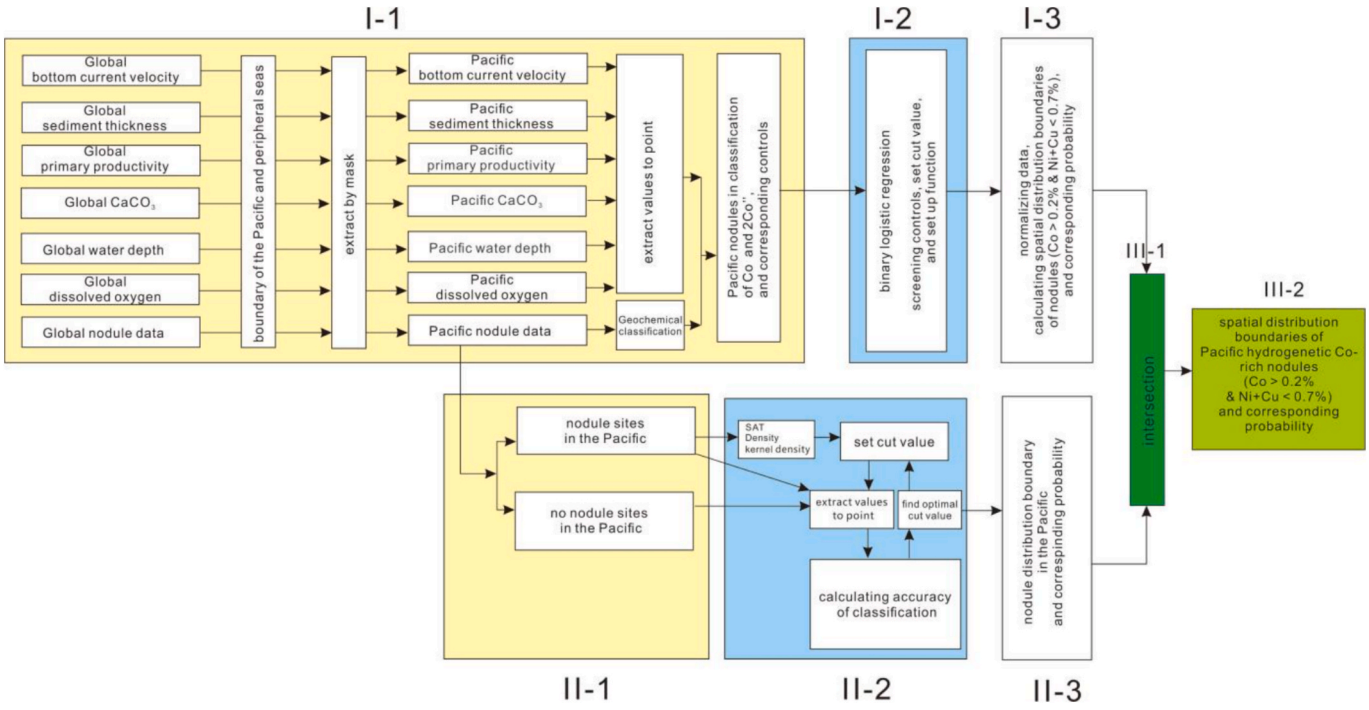

Fig. 2. Flowchart of this research on the distribution of Pacific hydrogenetic cobalt-rich nodules.

seawater, and recorded polymetallic nodule sites. Following the geochemical classification framework of deep-sea ferromanganese deposits proposed by Andreev (2020), polymetallic nodules from the world's three major oceans were categorized into five geochemical types based on their cobalt, nickel plus copper, and manganese contents (Table 1). These types comprise 2Co'' type, Co type, Ni–Cu–Co type, Ni–Cu type, and Mn type. In this research, nodules of the 2Co'' and Co types were identified as hydrogenetic cobalt-rich nodules, aligning with the classification of Bonatti et al. (1972) (Fig. 3), while the Ni–Cu–Co, Ni–Cu, and Mn types were grouped as non-hydrogenetic nodules. Additionally, the "Extract Values to Points" tool in ArcGIS was utilized to obtain data corresponding to the geographic coordinates of the Pacific nodule sites. This procedure extracted values from datasets representing bottom current velocity, sediment thickness, primary productivity, $CaCO_3$ concentration in surface sediments, water depth, and near-bottom dissolved oxygen content. The integrated results produced a comprehensive Pacific polymetallic nodule distribution dataset encompassing both the geochemical classifications of Pacific nodules and their associated ore-controlling environmental parameters.

I-2 Establishment of binary logistic regression equation

Using the Pacific polymetallic nodule distribution dataset, the ore-controlling factor data were normalized to remove the impact of scale differences among variables during correlation analysis. For the five controlling parameters, including bottom current velocity, sediment thickness, primary productivity, $CaCO_3$ content in surface sediments, and dissolved oxygen concentration in seawater, normalization was conducted by dividing each data value by its corresponding maximum value (normalized data = original data / maximum value). The respective maximum values used for normalization were 0.436 m s^{-1}, 7248 m, 2584 mg C m^{-2} day^{-1}, 25.826 g m^{-2} a^{-1}, and 263 μmol kg^{-1}. In contrast, water depth data were normalized according to the frequency of hydrogenetic cobalt-rich nodule occurrences within specific depth intervals (Fig. 4). Subsequently, a binary logistic regression equation was constructed to model the relationship between hydrogenetic cobalt-rich nodules and the selected ore-controlling parameters. Variables with p-values exceeding the established significance level in the Wald test were excluded from the model. The final regression equation retained four controlling parameters: water depth, sediment thickness, primary productivity, and dissolved oxygen concentration. Furthermore, a threshold (cut value) was determined based on the principle of optimizing the prediction accuracy for both hydrogenetic and non-hydrogenetic nodule classifications.

I-3 Hydrogenetic co-rich nodule distribution calculation

Using the binary logistic regression equation developed in step I-2

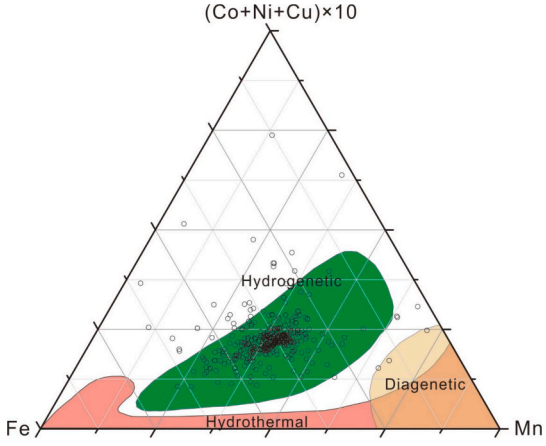

Fig. 3. Ternary discrimination diagram of Co type and 2Co'' type of nodules (Bonatti et al., 1972).

Table 1
Geochemical type of polymetallic nodules (modified after Andreev, 2020).

Geochemical Type	Contents %		
	Ni + Cu	Co	Mn
2Co'' type	0.3–0.7	>0.4	14.0–24.0
Co type	0.3–0.7	<0.4	15.0–21.0
Ni-Cu-Co type	0.7–1.7	<0.4	21.35–27.0
Ni-Cu type	>1.7	<0.4	25.0–33.0
Mn type	0.7–2.0	0.02–0.14	33.0–47.0

together with the Pacific polymetallic nodule distribution dataset from step I-1, the ore-controlling parameters (water depth, sediment thickness, primary productivity, and dissolved oxygen) were selected and normalized. With these normalized variables and the regression equation, the probability of hydrogenetic nodule occurrence across the Pacific was computed. The distribution range was then refined according to the defined cut value, and the probability (PA) of hydrogenetic Co-rich nodule occurrence within this range was established.

2.2.3. Kernel density estimation of hydrogenetic co-rich nodule distribution

II-1 data preparation

In the Pacific polymetallic nodule distribution research dataset, the sampling sites were categorized into those containing hydrogenetic Co-rich nodules and those without them.

II-2 Density analysis and threshold optimization

The spatial heat map of hydrogenetic Co-rich nodule distribution across the study area was generated using the "Kernel Density" tool in ArcGIS. A specific threshold was applied to delineate the distribution range of hydrogenetic Co-rich nodules. Subsequently, site data with and without hydrogenetic Co-rich nodules were processed using the "Extract Values to Points" tool in ArcGIS to obtain the corresponding density values for each location. The accuracy of the density map in distinguishing nodule types under the given threshold was then evaluated. The threshold was iteratively adjusted until the maximum classification accuracy and its corresponding value wereachieved, which was identified as the optimal threshold.

II-3 Calculation of Kernel density distribution of hydrogenetic cobalt-rich nodules

Using the optimal threshold obtained, the distribution range of hydrogenetic cobalt-rich nodules was delineated, and the probability (PB) of their distribution within this range was calculated. Subsequently, a kernel density distribution map of hydrogenetic Co-rich nodules in the Pacific was generated.

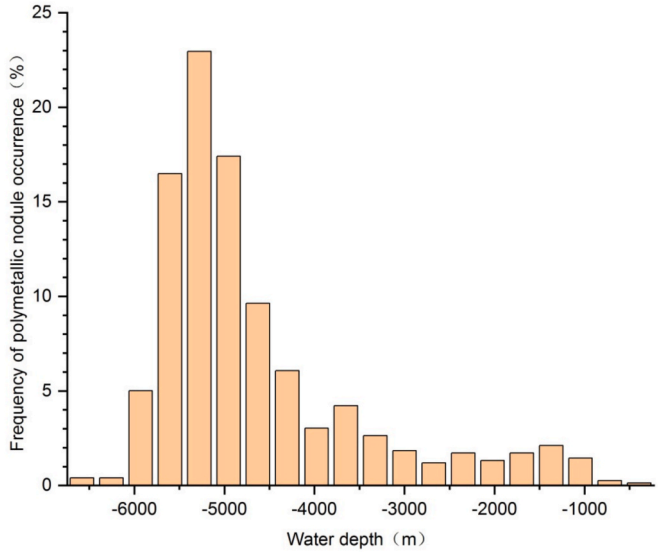

Fig. 4. Water depth frequency of Pacific polymetallic nodules occurrence.

2.2.4. Study on the distribution of APRA III-1 taking the intersection

To minimize the extent of the APRA, the prediction maps of Pacific hydrogenetic Co-rich nodules generated in steps I and II were intersected. When the sum of PA and PB is a constant value exceeding 100 %, and PA > PB, the probability range of hydrogenetic cobalt-rich nodule distribution within the intersection can be determined as [PA + PB − 1, PB].

III-2 Calculation of hydrogenetic cobalt-rich nodule distribution

Based on the overlap between the binary logistic regression prediction map and the kernel density distribution prediction map of hydrogenetic cobalt-rich nodules in the Pacific, the APRA was delineated. The probability of hydrogenetic cobalt-rich nodule distribution within this APRA falls within the range of [PA + PB − 1, PB].

3. Results

3.1. Results of binary logistic regression

Based on the obtained parameters of the binary logistic regression equation (Table 2), the following equation can be obtained:

$$P = \frac{1}{1 + \exp[-(\beta_0 + \beta_i x_i)]}$$

$$\beta_0 + \beta_i x_i = -1.868 - 1.335P\_WD\_N - 12.787P\_SeThick\_N - 26.016P\_PP\_N + 3.314P\_DO\_N$$

where P_WD_N is the normalized depth, P_SedThick_N represents the normalized sediment thickness, P_PP_N denotes the normalized primary productivity, and P_DO_N is the normalized dissolved oxygen content in the bottom water of the Pacific Ocean.

Applying a cut value of 0.08 in the binary logistic regression equation resulted in a prediction accuracy of 80.10 % for hydrogenetic cobalt-rich nodule sites, with 652 sites correctly identified and 162 misclassified. For non-hydrogenetic nodule sites, the prediction accuracy reached 77.87 %, with 9540 sites correctly predicted and 2711 misclassified, yielding an overall accuracy of 78.01 %.

The spatial distribution of hydrogenetic cobalt-rich nodules across the Pacific Ocean and its peripheral seas was derived from the regression model (Fig. 5). Under the Lambert Azimuthal Equal Area projection, regions exhibiting a cut value greater than 0.08 encompass a total area of 59,227,774 km^2. Within this zone, the probability of hydrogenetic cobalt-rich nodule occurrence remains relatively high at 78.01 %. Nonetheless, this region covers a substantial proportion (32.8 %) of the total study area, indicating a broad spatial extent of predicted nodule presence.

3.2. Results of kernel density analysis

By applying the "Kernel Density" tool in ArcGIS with a cut value of 0.05, the misjudgment rate for locations containing hydrogenetic Co-

Table 2
Variable parameters of the binary logistic regression equation.

	β	S.E.	Wald	df	Sig.	Exp(β)
P_WD_N	−1.335	0.488	7.491	1	0.006	0.263
P_SedThick_N	−12.787	2.288	31.229	1	0.000	0.000
P_PP_N	−26.016	1.322	387.257	1	0.000	0.000
P_DO_N	3.314	0.534	38.483	1	0.000	27.495
β_0	−1.868	0.404	21.433	1	0.000	0.154

Note: β: Coefficients of binary logistic regression equation; S.E.: Standard errors of β; Wald: Observations of wald statistics; df: Freedom; Sig.: Probabilities of wald statistics; Exp(β): Exp(β) = e^{β}.

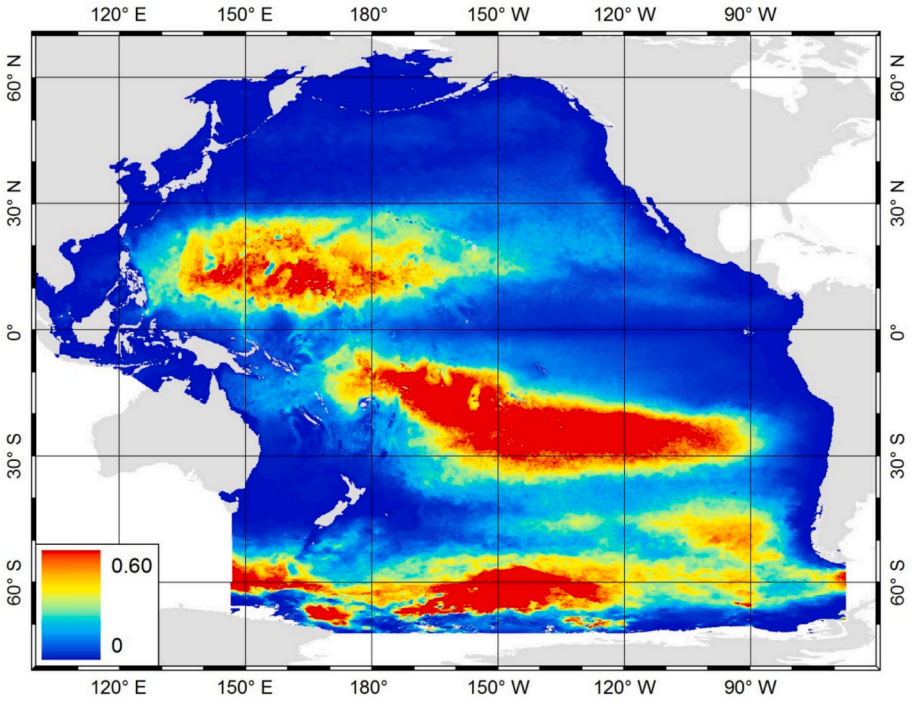

Fig. 5. Distribution of binary logistic regression for Pacific hydrogenetic Co-rich nodules (The red area means that it is highly probable to discover hydrogenetic Co-rich nodules, and vice versa).

Table 3
Cut values and corresponding misjudgments in kernel density analysis.

	Predicted site number by cut value		
cut value	0.03	0.04	0.05
HydrogeneticCo-rich nodules sites	814	774	760
non hydrogeneticCo-rich nodules sites	814	10,297	10,583
misjudgment rate for hydrogeneticCo-rich nodules sites	0.00 %	4.91 %	6.63 %
misjudgment rate for non hydrogeneticCo-rich nodules sites	93 %	16 %	14 %
Overall misjudgment rate	87.5 %	15.3 %	13.2 %

Note: The number of hydrogenetic cobalt-rich nodules sites is 814, and the number of non hydrogenetic cobalt-rich nodules sites is 12251.

rich nodules was determined to be 6.63 %, whereas the misjudgment rate for locations lacking such nodules was 14 %. This produced a total misjudgment rate of 13.2 % (Table 3).

The spatial distribution of hydrogenetic Co-rich nodules across the Pacific Ocean and its surrounding seas was derived through kernel density analysis using a cut value of 0.05 (Fig. 6). Based on the Lambert Azimuthal Equal Area projection, regions with values exceeding 0.05 encompass an area of 30,500,745 km^2. Within this region, the likelihood of hydrogenetic Co-rich nodule occurrence is notably high, reaching 86.8 %. Nevertheless, this area remains extensive, representing 16.9 % of the total study region.

3.3. Distribution of hydrogenetic cobalt-rich nodules in the Pacific Ocean

The total area of the Pacific Ocean and its peripheral seas considered in this study is 180,723,485 km^2. The APRA derived from binary logistic regression analysis covers 59,227,774 km^2, representing 32.8 % of the total study region, with a hydrogenetic cobalt-rich nodule distribution probability (P1) of 78.01 %. The APRA obtained through kernel density analysis encompasses 30,500,745 km^2, equivalent to 16.9 % of the study area, with a corresponding distribution probability (P2) of 86.8 %.

The comparison reveals that the APRAs identified by the two analytical approaches do not fully coincide. Notably, binary logistic regression predicts the presence of hydrogenetic cobalt-rich nodules in regions such as the East Pacific Rise, which are unsuitable for nodule formation (Hein et al., 2013), suggesting that the model exhibits a degree of overfitting. To refine the APRA delineation, the intersection of the two predictive results was taken (Fig. 7), yielding an area of 21,364,725 km^2, accounting for 11.8 % of the total study area. The estimated probability of hydrogenetic cobalt-rich nodule occurrence within this overlapping zone falls within the range [P1 + P2 − 1, min (P1, P2)], corresponding to values between 64.81 % and 78.01 %.

4. Discussion

4.1. Control mechanism of differentiating hydrogenetic nodules from diagenetic nodules

The geochemical characteristics of deep-sea ferromanganese deposits, including Mn, Co, Ni, and Cu contents, exhibit variations with water depth, which correspond to specific pH and dissolved oxygen ranges (Andreev, 2020; Chester and Jickells, 2009). Factors such as nanoparticle size, redox potential, and pH govern the valence state of Mn ions. As the redox potential increases, the Mn valence state transitions from +2 to +3 and eventually to +4 (Sun et al., 2019).Within 10 Å vernadite, Mn^{3+} preferentially occupies Jahn–Teller–distorted octahedral sites and plays a key role in the topotactic transformation to todorokite, ultimately contributing to todorokite stabilization in suboxic marine sediments (Manceau et al., 2014). This mineralogical transformation serves as an important distinction between Co-rich hydrogenetic nodules and diagenetic Ni–Cu–rich nodules. In hydrogenetic nodules, manganese minerals are predominantly composed of vernadite.

Compared with diagenetic nodules, hydrogenetic nodules exhibit an exceptionally high specific surface area, reaching up to 419 m^2/g (Ren et al., 2023). For interfacial reactions such as adsorption, the reaction rate can be expressed as $v = -\frac{dm}{dt} = k \bullet A \bullet C^n$, where v is the reaction rate, m is the reacting mass, t is time, k is a rate constant, A is the reaction interface area, C is the reactant concentration, and n is the

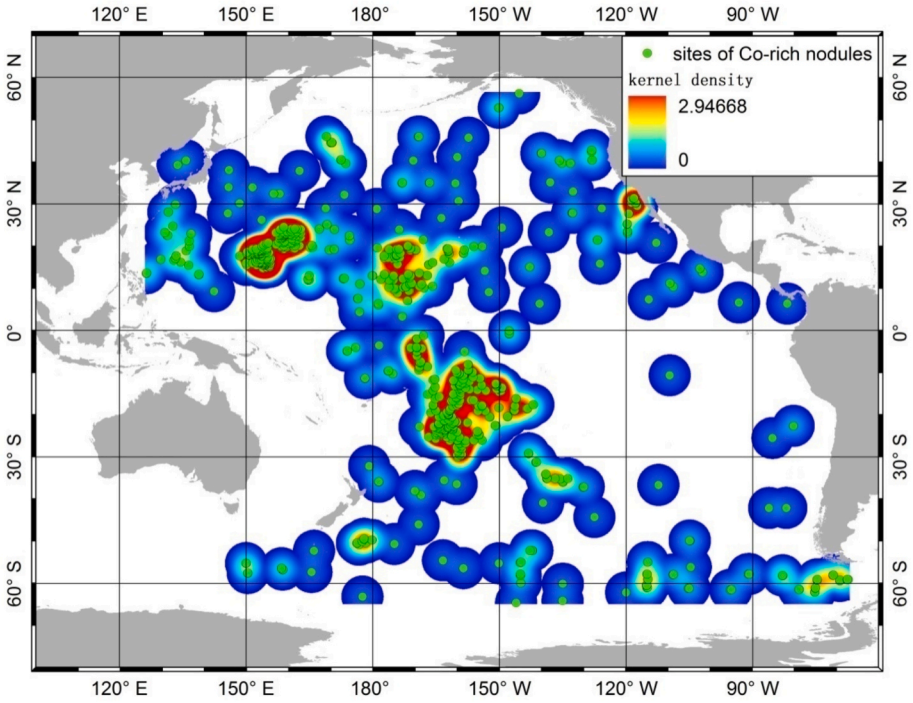

Fig. 6. Kernel density distributions of hydrogenetic cobalt-rich nodules in this study.

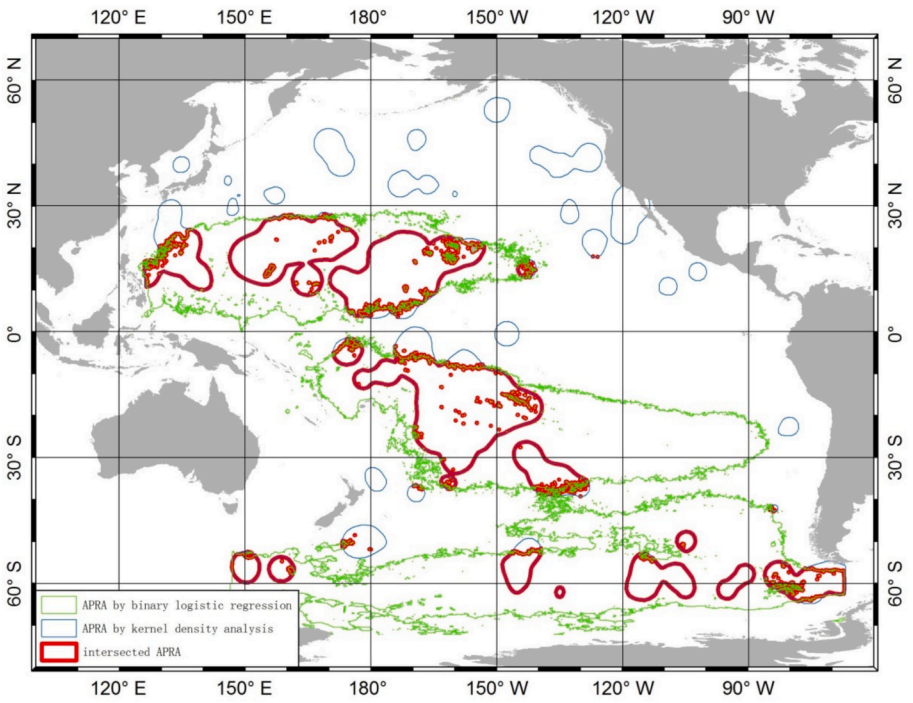

Fig. 7. Overlapping areas between the binary logistic regression distribution and the kernel density distribution of Pacific hydrogenetic cobalt-rich nodules.

reaction order. The large specific surface area of hydrogenetic nodules therefore enhances the adsorption of Co^{2+} from seawater onto vernadite surfaces. Additionally, within hydrogenetic nodules, Co^{2+} is oxidized to Co^{3+} by Mn^{3+} within the phyllomanganate buserite (Manceau et al., 1997), leading to a non saturation-controlled adsorption process. Consequently, the Co concentration in hydrogenetic nodules is also influenced by the duration of the adsorption reaction. In contrast, Ni and Cu are primarily derived from the dissolution of biogenic silica, calcium tests, or reduced organic matter (Chester and Jickells, 2009), which regulate the concentrations of adsorbed species.

The occurrence of hydrogenesis or diagenesis in deep-sea environments is primarily influenced by pH and dissolved oxygen conditions. These factors are determined by the transport of oxygenated seawater near the seafloor through bottom currents, such as the Antarctic Bottom Water, and by the reduction of organic matter that settles onto the seafloor from the overlying water column, particularly from surface waters (Koschinsky and Hein, 2003; Halbach et al., 1988; Koschinsky and Halbach, 1995). Consequently, the spatial distribution of

hydrogenetic nodules can be effectively predicted by integrating parameters such as surface primary productivity, dissolved oxygen levels near the seabed, bottom current dynamics, water depth, and $CaCO_3$ concentrations in surface sediments.

4.2. Control factors for predicting distribution of hydrogenetic cobalt-rich nodules

The spatial distribution of hydrogenetic cobalt-rich nodules is influenced by multiple environmental and geological parameters (Dutkiewicz et al., 2020; Kuhn et al., 2017), such as sediment thickness, surface primary productivity, $CaCO_3$ concentration in sediments, dissolved oxygen levels in seawater, water depth related to bottom water formation, and bottom current velocity. When sediment flux is elevated, as observed in certain marginal sea basins, thick sediment layers accumulate and induce a dilution of cobalt within nodules (Ren et al., 2024), thereby reducing their cobalt content. Elevated primary productivity promotes the deposition of organic materials that subsequently decompose, triggering diagenetic processes (Andreev, 2020; Chester and Jickells, 2009), which suppress cobalt enrichment in the nodules. Increased $CaCO_3$ concentration in sediments reflects a greater input of biogenic material, unfavorable for nodule formation, since the carbonate compensation depth (CCD) exerts a critical influence on nodule development (Kuhn et al., 2017). Furthermore, reduced dissolved oxygen in bottom waters indicates an environment favoring diagenetic alteration rather than the precipitation of hydrogenetic cobalt-rich nodules (Александров, 2009; Chester and Jickells, 2009).

The regression coefficients obtained from the binary logistic regression analysis indicate that sediment thickness and primary productivity, with values of −12.787 and −26.016 respectively, are the predominant factors influencing the spatial distribution of cobalt-rich nodules in the Pacific Ocean. The spatial resolution of sediment thickness and primary productivity datasets employed in this study enables the differentiation of hydrogenetic Co-rich nodules from other nodule types across the Pacific region, which likely explains their dominant control on nodule distribution. The water depth dataset was adjusted according to the frequency of polymetallic nodule occurrence within specific depth intervals, revealing a correlation with hydrogenetic Co-rich nodules and yielding a regression coefficient of −1.335. In contrast, the dissolved oxygen data, sourced from global profiles (https://www.ewoce.org), have spatial intervals on the order of several degrees, which limit their ability to effectively distinguish hydrogenetic nodules from other nodule types. Consequently, the regression coefficient for dissolved oxygen is relatively low at 3.314. Although both bottom current velocity and $CaCO_3$ concentration in sediments are theoretically associated with cobalt nodule formation (Kuhn et al., 2017; Chester and Jickells, 2009; Александров, 2009), their regression coefficients are effectively zero and negligible, possibly due to their weaker discriminative capability compared to sediment thickness and primary productivity.

Although correlation-based approaches such as binary logistic regression are valuable for predicting the spatial distribution of hydrogenetic cobalt-rich nodules, their effectiveness is constrained by the types of available data and their spatial resolution. Consequently, instances of overfitting may occur, as evidenced by the predicted nodule distribution near the East Pacific Rise (Fig. 5), which contradicts geological models indicating that nodules primarily form in deep ocean basins (Hein et al., 2013). To address this limitation, the present study integrated binary logistic regression with kernel density analysis, which relies solely on geological observation data (Fig. 6). This combined approach effectively mitigates the overfitting observed in the southeastern Pacific (Fig. 7), while also filtering out certain anomalous data points from geological observations (Fig. 6). These outcomes demonstrate the importance of integrating data-driven statistical techniques with geological understanding to achieve more reliable predictions of hydrogenetic cobalt-rich nodule distribution.

5. Conclusion

Hydrogenetic cobalt-rich nodules in the Pacific Ocean are predominantly concentrated in the low-latitude waters of the western Pacific, particularly within the Mariana Basin, the Philippine Basin, the northern sector of the Central Pacific Basin, and the northern portion of the Southwest Pacific Basin. Additionally, cobalt-rich nodules are also observed in the Southern Ocean near 60 degrees south latitude. The formation and spatial distribution of hydrogenetic cobalt-rich nodules are governed by multiple environmental and geological parameters, including sediment thickness, primary productivity, $CaCO_3$ content in sediments, dissolved oxygen concentration in seawater, water depth, and bottom current velocity. Results from binary logistic regression indicate that sediment thickness and primary productivity are the dominant factors influencing nodule formation, suggesting their effectiveness as key predictors for mapping the distribution of hydrogenetic Co-rich nodules. Moreover, reliable prediction of nodule distribution requires the integration of statistical modeling techniques with geological insights to capture both data-driven patterns and geologically constrained controls.

Funding

This work financially supported by the Marine S&T Fund of Shandong Province for Laoshan Laboratory [grant number: LSKJ202203600-2], and by the China Ocean Mineral Resources R&D Association (COMRA) project [grant number: DY135-N2-1-04].

Declaration of competing interest

The authors declare that they have no known competing financial interests or personal relationships that could have appeared to influence the work reported in this paper.

Data availability

The authors do not have permission to share data.

References

Andreev, S.I., Anikeeva, L.I., Ivanova, A.M., Krasny, L.I., Yubco, V.M., Uglov, B.D., 2004. Mineragenetic map of the world ocean (1:15 000 000). St. Petersburg: FSBI VNIIOCEANGEOLOGIA.

Andreev, S.I., 2020. Principles of ocean metallogeny. Geol. Polezn. Iskop. Mirovogo Okeana 16 (2), 3–23. https://doi.org/10.15407/gpimo2020.02.003.

Bonatti, E., Kraemer, T., Rydell, H., 1972. Classification and genesis of submarine iron-manganese deposits. In: Horn, D.R., editor. Ferromanganese deposits on the ocean floor. Washington D.C.: Natl. Sci. Found, 159-66.

Bouabdellah, M., Maacha, L., Levresse, G., Saddiqi, O., 2016. The BouAzzer Co-Ni-Fe-As (±Au ± Ag) district of Central Anti-Atlas (Morocco) — a long-lived late Hercynian to Triassic magmatic-hydrothermal to low-sulphidation epithermal system. In: Bouabdellah, M., Slack, J.F. (Eds.), Mineral Deposits of North Africa. Springer-Verlag, Berlin, pp. 229–247. https://doi.org/10.1007/978-3-319-31733-5_8.

Chester, R., Jickells, T., 2009. Marine geochemistry. John Wiley and Sons https://doi.org/10.1002/9781118349083.

Cronan, D.S., 1967. The geochemistry of some manganese nodules and associated pelagic deposits [dissertation]. London: Imperial College of Science and Technology.

Dutkiewicz, A., Judge, A., Müller, R.D., 2020. Environmental predictors of deep-sea polymetallic nodule occurrence in the global ocean. Geology 48, 293–297. https://doi.org/10.1130/G46836.1.

Flanders Marine Institute. IHO Sea Areas, version 3 [Internet]. 2018 [cited 2018 Oct 12]. Available from: https://www.marineregions.org/.https://doi.org/10.14284/323.

Frazer J, Fisk M., 1981. Scripps Institution of Oceanography Ferromanganese Nodule Analysis File - IDOE Portion. National Geophysical Data Center, NOAA. https://doi.org/10.7289/V5TB14TS.

Halbach, P., Friedrich, G., von Stackelberg, U., 1988. The manganese nodule belt of the Pacific Ocean. Stuttgart, Germany: Ferdinand EnkeVerlag. https://doi.org/10.1180/minmag.1989.053.373.33.

Hein, J.R., Koschinsky, A., Kuhn, T., 2020. Deep-ocean polymetallic nodules as a resource for critical materials. Nat. Rev. Earth Environ. 1, 158–169. https://doi.org/10.1038/s43017-020-0027-0.

Hein, J.R., Spinardi, F., Okamoto, N., Mizell, K., Thorburn, D., Tawake, A., 2015. Critical metals in manganese nodules from the Cook Islands EEZ, abundances and distributions. Ore Geol. Rev. 68, 97–116. https://doi.org/10.1016/j.oregeorev.2014.12.011.

Hein, J.R., Mizell, K., Koschinsky, A., Conrad, T.A., 2013. Deep-ocean mineral deposits as a source of critical metals for high- and green-technology applications: Comparison with land-based resources. Ore Geol. Rev. 51, 1–14. https://doi.org/10.1016/j.oregeorev.2012.12.001.

Herrington, R.J., Zaykov, V.V., Maslennikov, V.V., Brown, D., Puchkov, V.N., 2005. Mineral deposits of the Urals and links to geodynamic evolution. Econ. Geol. 100th Anniversary Volume, 1069-95. https://doi.org/10.5382/av100.32.

Koschinsky, A., Halbach, P., 1995. Sequential leaching of marine ferromanganese precipitates: Genetic implications. Geochim. Cosmochim. Acta 59, 5113–5132. https://doi.org/10.1016/0016-7037(95)00358-4.

Koschinsky, A., Hein, J.R., 2003. Uptake of elements from seawater by ferromanganese crusts: Solid-phase associations and seawater speciation. Mar. Geol. 198, 331–351. https://doi.org/10.1016/S0025-3227(03)00122-1.

Kuhn, T., Wegorzewski, A., Rühlemann, C., Vink, A. Composition, Formation, and Occurrence of Polymetallic Nodules. Springer International Publishing, 2017. https://doi.org/10.1007/978-3-319-52557-0_2.

Oregon State University. Ocean Productivity [Internet]. [cited 2020 Feb 11]. Available from: http://science.oregonstate.edu/ocean.productivity/index.php.

International Seabed Authority.[Internet]. 2010 [cited 2010 Aug 26]. Available from: http://www.isa.org.jm/.

Jiao, J.-G., Huang, X.-F., Yuan, H.-C., Chen, B., Sun, T., Liu, R.-P., 2009. New progress in research on the De'erni copper (cobalt) deposit in Qinghai Province. J. Earth Sci. Environ. 31 (1), 42–47. https://doi.org/10.3969/j.issn.1672-6561.2009.01.004. InChinese.

Manceau, A., Drits, V.A., Silvester, E., Bartoli, C., Lanson, B., 1997. Structural mechanism of Co^{2+} oxidation by the phyllomanganate buserite. Am. Mineral. 82, 1150–1175. https://doi.org/10.2138/am-1997-11-1213.

Manceau, A., Lansin, M., Takahashi, Y., 2014. Mineralogy and crystal chemistry of Mn, Fe, Co, Ni, and Cu in a deep-sea Pacific polymetallic nodule. Am. Mineral. 99, 2068–2083. https://doi.org/10.2138/am-2014-4742.

Mero, J.L., 1965. The Mineral Resources of the Sea (oceanography Series vol. 1. https://doi.org/10.1016/s0422-9894(08)70759-1.

Mizell, K., Hein, J.R., Au, M., Gartman, A., 2022. Estimates of Metals Contained in Abyssal Manganese Nodules and Ferromanganese Crusts in the Global Ocean Based on Regional Variations and Genetic Types of Nodules. In: Sharma, R. (eds) Perspectives on Deep-Sea Mining. Springer, Cham. https://doi.org/10.1007/978-3-030-87982-2_3.

Monget, J.M., Murry, J.W., Mascle, J., 1976. A world-wide compilation of published, multicomponent analyses of ferromanganese concretions. https://doi.org/10.13140/2.1.4671.5680.

Peltonen, P., Kontinen, A., Huhma, H., Kuronen, U., 2008. Outokumpu revisited: New mineral deposit model for the mantle peridotite-associated Cu-Co-Zn-Ni-Ag-Au sulphide deposits. Ore Geol. Rev. 33 (3–4), 559–617. https://doi.org/10.1016/j.oregeorev.2007.07.002.

Peter, J.M., Scott, S.D., 1997. Windy Craggy, northwestern British Columbia: The world's largest besshi-type deposit. Rev. Econ. Geol. 8, 261–295. https://doi.org/10.5382/Rev.08.12.

Prokin, V.A., Buslaev, F.P., 1998. Massive copper-zinc sulphide deposits in the Urals. Ore Geol. Rev. 14 (1), 1–69. https://doi.org/10.1016/s0169-1368(98)00014-6.

Ren, X.-W., Li, H.-N., Yan, S.-J., Li, H.-M., Shi, X.-F., 2023. Hydrogenetic and diagenetic controls on the specific surface area of polymetallic nodules in deep ocean basins. Minerals 13, 1431. https://doi.org/10.3390/min13111431.

Ren, X.-W., Hein, J.R., Yang, Z.Z., Xing, N., Zhu, A.M., 2024. Controls on cobalt concentrations in ferromanganese crusts from the Magellan seamounts, west Pacific. Front. Mar. Sci. 11, 1489943. https://doi.org/10.3389/fmars.2024.1489943.

Straume, E.O., Gaina, C., Medvedev, S., Hochmuth, K., Gohl, K., Whittaker, J.M., Abdul Fattah, R., Doornenbal, J.C., Hopper, J.R., 2019. GlobSed: Updated total sediment thickness in the world's oceans. Geochem. Geophys. Geosyst. 20. https://doi.org/10.1029/2018gc008115.

Sulpis, O., Boudreau, B.P., Mucci, A., Key, R.M., 2018. Current $CaCO_3$ dissolution at the seafloor caused by anthropogenic CO_2. Proc. Natl. Acad. Sci. USA 115 (31), 7949–7954. https://doi.org/10.1073/pnas.1804250115.

Sun, W.-H., Kitchaev, D.A., Kramer, D., Ceder, G., 2019. Non-equilibrium crystallization pathways of manganese oxides in aqueous solution. Nat. Commun. 10 (1), 1–9. https://doi.org/10.26434/chemrxiv.6300959.

U.S. Geological Survey, 2024. Mineral commodity summaries 2024: U.S. Geological Survey, 212 p. https://doi.org/10.3133/mcs2024.

von Stackelberg, U., 1997. Growth history of manganese nodules and crusts of the Peru Basin. In: Hicholson, K., Hein, J.R., Buhn, B., Dasgupta, S., editors. Manganese mineralization: Geochemistry and mineralogy of terrestrial and marine deposits. Geological Society Special Publication No. 119, 153-76. https://doi.org/10.1144/gsl.sp.1997.119.01.11.

Wang, Z.-L., Xu, D.-R., Chi, G.-X., Shao, Y.-J., Lai, J.-Q., Deng, T., Guo, F., Wang, Z., Dong, G.-J., Ning, J.-T., Zou, S.-H., 2017. Mineralogical and isotopic constraints on the genesis of the Jingchong Co-Cu polymetallic ore deposit in northeastern Hunan Province. South China. Ore Geol. Rev. 88, 638–654. https://doi.org/10.1016/j.oregeorev.2017.02.011.

Williams, P.J., Pollard, P.J., 2001. Australian Proterozoic iron oxide-Cu-Au deposits: An overview with new metallogenic and exploration data from the Cloncurry district, northwest Queensland. Explor. Min. Geol. 10 (3), 191–213. https://doi.org/10.2113/0100191.

World Ocean Circulation Experiment (WOCE) [Internet]. [cited 2020 Nov 2]. Available from: www.ewoce.org.

General Bathymetric Chart of the Oceans (GEBCO) [Internet]. [cited 2013 Sep 30]. Available from: www.gebco.net.

Yu, J.-J., Mao, J.-W., Chen, F.-X., Wang, Y.-H., Che, L.-R., Wang, T.-Z., Liang, J., 2014. Metallogeny of the Shilu Fe-Co-Cu deposit, Hainan Island, South China: Constraints from fluid inclusions and stable isotopes. Ore Geol. Rev. 57, 351–362. https://doi.org/10.1016/j.oregeorev.2013.08.018.

Zhu, Z.-M., Li, T.-X., Chen, L., Tan, H.-Q., Liu, Y.-D., 2014. Sulfur isotope geochemistry of Lala IOCG deposit in Sichuan province. Geol. J. China Univ. 20 (1), 28–37. https://doi.org/10.3969/j.issn.1006-7493.2014.01.003. In Chinese.

Zou, S.-H., Zou, F.-H., Ning, J.-T., Deng, T., Yu, D.-S., Ye, T.-W., Xu, D.-R., Wang, Z.-L., 2018. A stand-alone Co mineral deposit in northeastern Hunan Province, South China: Its timing, origin of ore fluids and metal Co, and geodynamic setting. Ore Geol. Rev. 92, 42–60. https://doi.org/10.1016/j.oregeorev.2017.11.008.

Александров, П.А., Аникеева, Л.И., Андреев, С.И., ПеМухов, С.И., 2009. ТалассохиМия рудогенеза Мирового океана. Санкт-Петербург. (In Russian).